14th International Conference on Applications of Statistics and Probability in Civil Engineering, ICASP14
Dublin, Ireland, July 9-13, 2023

Prediction of diaphragm wall displacements using Bayesian model calibration

Jocelyn MININI
Research Engineer, HES-SO // University of Applied Sciences Western Switzerland, School of Engineering and Architecture (HEIA-FR)

Stéphane COMMEND
Professor, HES-SO // University of Applied Sciences Western Switzerland, School of Engineering and Architecture (HEIA-FR)

ABSTRACT: This contribution presents a probabilistic and Bayesian approach for the finite element modelling of a deep excavation in a lacustrine environment in Geneva, Switzerland. Coupling non-linear 3D finite element modeling with highly accurate meta-modelling techniques was shown to be necessary in order to run time requiring analyses like Sobol' sensitivity and Monte-Carlo reliability analyses. A priori input parameters' probability density functions were based on geotechnical site tests, literature and our expertise. Displacement measurements from on-site monitoring were subsequently used during the first excavation phases in order to conduct an inverse Bayesian analysis. This helped us to refine our prior knowledge for final settlements' probability density functions and associated failure probabilities. In particular, the need to install the fourth level of bracing has been evaluated in the light of this risk analysis.

1. INTRODUCTION

The construction of an administrative centre is planned in Geneva. The project involves the execution of a large excavation in soft clays, with a maximum excavation level of about -18 m. The designed retaining system comprises a one-meter thick slurry wall supported by three to four levels of struts. 2D and 3D finite element analyses have been conducted with ZSOIL (2023) to evaluate the excavation's influence on the neighbouring structures and check the design forces in the wall and the struts. As Commend et al. (2004) have shown, the pore-water pressure change is one of the main factors influencing the behaviour of deep excavations in such soft and saturated soils: taking into account 100% of pore-pressures in 2D permanent drained analyses often leads to an overshoot in the prediction of displacements and associated forces in the support system, as the reality is 3D and transient (partially drained). In the specific context of the Geneva region, the study of piezometers has also shown that during underground works, soil decompression leads to a drop in the pore-water pressures that can reach 20 to 40%. With this in mind, a probabilistic framework has been put into place to evaluate the need to place a fourth level of bracing in the deepest part of the excavation. First, sensitivity analysis allows us to concentrate on the most relevant input parameters. Then, a priori distributions of pore pressures and soils' geotechnical parameters – taken from the geotechnical report as well as our experience – are propagated through our computational model, yielding probability density functions for the most significant results (horizontal displacement of the wall, settlements, bending moments). Finally, an inverse Bayesian analysis, based on displacements measured from inclinometers after the installation of the first level of struts, allows us to refine the input parameters' distributions and therefore predict with better accuracy the

behaviour of the subsequent excavation steps. It has to be noted that this paper has been written before the excavation was completed: displacements corresponding to the full excavation are not known by the authors but should be available in time for presentation during the conference.

2. METHODS AND TOOLS

The current probabilistic analysis is driven by the coupling between ZSOIL (2023) and the uncertainties quantification framework UQLab (Marelli and Sudret (2014)). According to the general scheme proposed by Sudret (2007) and de Rocquigny et al. (2008), methods such as meta-modelling, sensitivity analyses, Monte-Carlo analyses and Bayesian inference are used in this paper. This section proposes an overview of these methods.

2.1. Numerical model

Let us define $\mathcal{M}$ as a model which describes a geomechanical problem:

$$\boldsymbol{X} \in \mathcal{D}_X \subset \mathbb{R}^M \mapsto Y = \mathcal{M}(\boldsymbol{X}) \in \mathbb{R} \tag{1}$$

where $\boldsymbol{X} = \{x_1, ..., x_M\}$ is the matrix including the M input parameters and Y, the output quantity also called QoI (Quantity of Interest). If multiple quantities of interest are considered, $\boldsymbol{Y} \in \mathbb{R}^q$ is defined as a vector with q components. In the current article, $\mathcal{M}$ represents a ZSOIL finite element model which is tasked to solve the following system of partial differential equations:

$$\mathcal{M}: \begin{cases} (\sigma_{ij} + S\ P\ \delta_{ij})_{,j} + f_i & = 0 \\ -k_{ij}\ k_r(S) \left(-\dfrac{p}{\gamma_f} + H \right)_{,j} & = 0 \end{cases} \tag{2}$$

Eq. (2) involves a two-phase analysis with stationary flow or steady-state flow. The constitutive behaviour of soils is modelled by the hardening soil model with the brick-formulation (Cudny and Truty (2020)).

2.2. Approximation model

Due to the large number of model evaluations when coupling probabilistic analyses and finite elements method, an approximation model or meta-model must be created. Schöbi (2019) showed that the coupling between polynomial fitting and Gaussian process techniques could catch the global and local behaviour of the model being approximated, finally achieving a precise meta-model. This family of meta-models is called *Polynomial Chaos Kriging* and is defined by combining a set of orthonormal polynomials $\Psi_{\alpha}(\boldsymbol{X})$, which describes the trend of the Kriging, and the zero-mean, unit-variance stationary Gaussian process $\sigma^2 Z(\boldsymbol{X}, \omega)$ as follows :

$$\widehat{\mathcal{M}}_{\mathrm{PCK}}(\boldsymbol{X}) = \sum_{\alpha \in \mathcal{A}} y_{\alpha} \Psi_{\alpha}(\boldsymbol{X}) + \sigma^2 Z(\boldsymbol{X}, \omega) \tag{3}$$

In this paper, PCK-meta-models are considered for the probabilistic analyses. The training points set $\mathcal{Y}$, which allows the creation of a meta-model is commonly called *Experimental Design* or *ED*. It is made of the i original model responses:

$$\mathcal{Y} \supset Y_i = \mathcal{M}(\boldsymbol{X}_i) \tag{4}$$

2.3. Sensitivity analysis

In numerical modelling, identifying key model parameters allows more accuracy in calculations and may help the modeller identify the impacting variables on the model response. Driving such sensitivity analyses may help set the non-impacting parameters as deterministic variables while impacting variables can be kept as probabilistic distributions. Reconsidering Eq. (1), Sobol' indices (Sobol (2001)) describe how the variability of input parameters impacts the output model response. The first and higher Sobol' indices are defined by the Eq. (5) where D is the total variance and $D_{i_1,...,i_s}$ the partial variances of a model response. Eq. (6) yields then the total Sobol' indices.

$$S_{i_1,...,i_s} = \frac{D_{i_1,...,i_s}}{D} \tag{5}$$

$$S_i^T = \sum_{i \subset \{i_1,...,i_s\}} S_{i_1,...,i_s} \tag{6}$$

2.4. Reliability analysis

Here, reliability analyses are driven by Monte-Carlo simulations (MCS). By introducing a $g(\boldsymbol{X})$ function which represents an hypersurface bounding the *safe* and the *failure* domain, the *indicator function of the failure domain*:

$$\mathbf{1}_{\mathcal{D}_f}(\boldsymbol{x}) = \begin{cases} 1 & \text{if } g(\boldsymbol{x}) \leq 0 \\ 0 & \text{if } g(\boldsymbol{x}) > 0 \end{cases}, \boldsymbol{x} \in \mathcal{D}_{\boldsymbol{X}} \quad (7)$$

provides a method to compute a probability of failure numerically by MCS. This probability is called the empiric probability of failure, is exact when the number of model evaluation $N \to \infty$ and is given by

$$\widehat{P}_f = \frac{1}{N}\sum_{k=1}^{N} \mathbf{1}_{\mathcal{D}_f}\left(\boldsymbol{x}^{(k)}\right) = \frac{N_{fail}}{N} \quad (8)$$

2.5. Bayesian analysis

When performing Bayesian analyses, Eq. (1) must be extended by an additive model discrepancy to link the predictions with field measurement data. Assuming that this discrepancy term is normally distributed, with zero-mean value and with SD Σ, a prediction is given by Eqs. (1) and (3) :

$$Z \approx Y + \varepsilon \approx \widehat{\mathcal{M}}_{\text{PCK}}(\boldsymbol{X}) + \varepsilon \quad \text{where} \quad \varepsilon = \mathcal{N}(0, \Sigma) \quad (9)$$

Considering the additive discrepancy given in Eq. (9) and according to Bayes' theorem, the calculation of the distribution of the input *given* one measurement z_i is performed by

$$f_{\boldsymbol{X}}(\boldsymbol{X} \mid Z) = a \cdot f_{\boldsymbol{X}}(\boldsymbol{X}) \cdot \prod_{i=1}^{N} \mathcal{N}(z_i \mid \widehat{\mathcal{M}}_{\text{PCK}}(\boldsymbol{X}), \boldsymbol{\Sigma}) \quad (10)$$

where $a^{-1} = \int_{-\infty}^{\infty} \mathcal{L}(x) f_{\boldsymbol{X}}(x) dx$ is the normalizing constant. Bayesian analyses performed later in the present article are numerically solved by the Markov Chain Monte Carlo algorithm implemented in UQLab. The sampling method used for the chains construction is the Adaptive Metropolis algorithm (AM) (Wagner et al. (2021)).

3. STUDY CASE DESCRIPTION

To pursue the development of its activities, the Pictet Group has decided to construct an avant-garde building at the heart of the major Praille Acacias Vernets urban development project in Geneva Switzerland (**GoogleEarth**). The Campus Pictet de Rochemont aims to become one of the most emblematic building complex of the Praille Acacias Vernets project. It will be also an environmental reference in its construction concept, energy consumption and accessibility, with a strong emphasis on car-free living (Pictet Group (2023). The part of the project studied in this article is a vertical slice of a 17.3 meters high diaphragm wall. The calculations are not presented retrospectively, which means that the excavation was not yet at its final level when this paper was prepared.

3.1. Geometry and excavation stages

The geometry of the 4.32 meters width slice is well described in Fig. 1. The 17.3 meters high 'trouser legs' (see legend Fig. 1) diaphragm wall is built in C30/37 reinforced concrete with one-meter thickness. Three to four circular ROR-type struts are planned for the horizontal stabilisation of the wall. Four excavation stages are defined in Figs. 1b to 1e on which inclinometer monitoring is planned. In the current project, only stage S26 (Fig. 1c) was considered because of the availability of the measurements. A sensitive water pipe is situated a few meters before the excavation area (Fig. 1a). Movements in this area are only tolerated beneath a specific threshold (see Tab. 4).

Table 1: Hardening Soil Model parameters.

Formation	**Stiffness**		**Strength**			**Stress state**				
	$E_{50} = E_{\text{oed}}$ (MPa)	E_{ur} (MPa)	φ (°)	ψ (°)	c (kPa)	K_0 (-)	OCR (-)	σ_{ref} (kPa)	$\sigma_{\text{oed,ref}}$ (kPa)	m (-)
Fill	15	60	33	3	1	0.46	1.0	9	20	0.5
Alluvium	50	150	40	10	0	0.36	1.0	22	62	0.5
FC-Wurm retreat	7	32	30	0	7	0.50	1.0	95	190	0.5
WC-Wurm retreat	18	54	31	1	17	0.48	1.0	96	200	0.5
Moraine	50	150	35.5	5.5	21	0.42	2.0	84	200	0.5

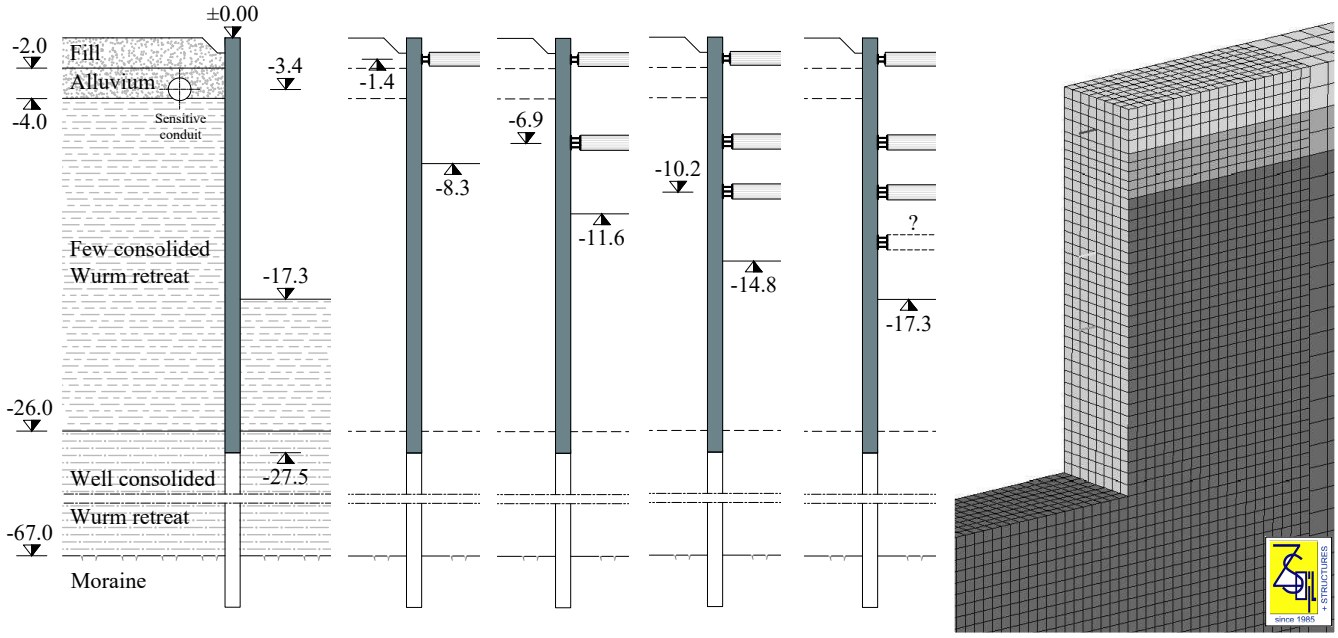

(a) Stratigraphy (b) S26 (c) S33 (d) S43 (e) S50 (f) FE Model

Figure 1: (a) Diaphragm wall at its final stage with its corresponding stratigraphy. (b to e) Excavation stages with ROR struts. (f) Isometric view of the 3D slice model on ZSOIL. The change in colour of the wall represents the boundary between the continuous and the 'trouser legs' part.

3.2. Quantities of interest

Referring to Eq. (1), three quantities of interest were defined for the purposes of the study: horizontal wall deflection U_x; the vertical displacement U_y of the sensible water conduit; the maximal bending moment M of the wall. This involves $\boldsymbol{Y} \in \mathbb{R}^3$.

3.3. Soil properties

The stratigraphy is described in Fig. 1a. It consists of 5 soil layers, two of which could be problematic. The Wurm retreats were identified as sandy and clayey silts with weak strength and deformability proprieties. The mean geomechanical properties are given in Tab. 1. One of the particularities of Geneva soils is the loss of pore pressure during a change of stress state. This pressure drop is difficult to be captured by a decoupled model. To try to capture this effect, we considered the water pressure in ZSOIL as a random variable. The probabilistic characterization of the problem is described in the next section.

3.4. Uncertainties quantification

Here, uncertainties quantification is understood as the establishment of a list of parameters being treated as a random vector described by a joint density probability function $\boldsymbol{X} \sim f_{\boldsymbol{X}}$. The statistical distributions of soil parameters and the coefficients of variation were established according to the literature (Phoon and Ching (2018),TG-C3 (2023)), whereas the mean values of the distributions were defined according to Tab. 1. The relationship between the secant and the unloading-reloading

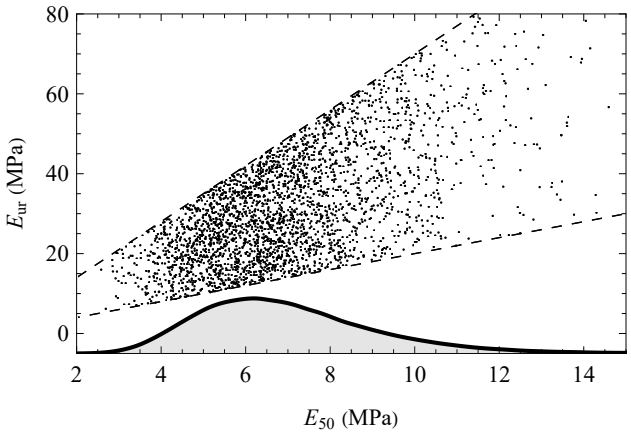

Figure 2: Relationship between E_{50} and E_{ur} through Γ_{ur}. Dashed lines represent the boundaries of the uniform distribution.

modulus was introduced by a scalar Γ_{ur} uniformly distributed between 2 and 7 as shown in Fig. 2. Such values are commonly encountered (Obrzud and Truty (2010)). The pore pressure loss was introduced by considering a multiplier of the water weight γ_w denoted as κ_w. We regarded this factor as being uniformly distributed between 35% and 85% based on our experience on other neighbouring projects. The quantification led to an input of 18 random variables. The distributions families are described in Tab. 2. This initial input may be reduced by driving a sensitivity analyses as described in section 2.3.

Table 2: Statistical distributions and their moments

Parameter	f_X	Parameters or CV
Friction angle	$\mathcal{LN}$	CV = 10%
Cohesion	$\mathcal{LN}$	CV = 20%
Young-modulus	$\mathcal{LN}$	CV = 30%
Γ_{ur}	$\mathcal{U}$	(2,7)
Water table depth	$\mathcal{N}$	(3.6, 0.05)
Water pressure κ_w	$\mathcal{U}$	(0.35, 0.85)

3.5. *Monitoring and model discrepancy*

According to Eq. (9), using a predictor model requires the addition of a discrepancy term. We chose to separate the measurement error $\boldsymbol{\varepsilon}_{\mathcal{Z}}$, the original model error $\boldsymbol{\varepsilon}_{\mathcal{M}}$ and the meta-model error $\boldsymbol{\varepsilon}_{\widehat{\mathcal{M}}}$:

$$\boldsymbol{\varepsilon} = \boldsymbol{\varepsilon}_{\mathcal{Z}} + \boldsymbol{\varepsilon}_{\mathcal{M}} + \boldsymbol{\varepsilon}_{\widehat{\mathcal{M}}} \tag{11}$$

$\boldsymbol{\varepsilon}_{\mathcal{Z}}$ was quantified as the accuracy obtained from the inclinometer surveys and as the error generated by smoothing the noisy measurement data (Fig. 7). Considering a confidence interval of 5% resp. 95% on the accuracy of the measurements (given as ±1 mm), the resulting standard deviation yields $\boldsymbol{\sigma}_{\boldsymbol{\varepsilon}_{\mathcal{Z}}} = \mathbf{1.0}$.

$\boldsymbol{\varepsilon}_{\mathcal{M}}$ was selected based on personal judgement. The error was correlated to the magnitude of the measured settlements with a coefficient of variation $\mathrm{CV}_{\boldsymbol{\varepsilon}_{\mathcal{M}}} = 0.20 \rightarrow \boldsymbol{\sigma}_{\boldsymbol{\varepsilon}_{\mathcal{M}}} = \mathrm{CV}_{\boldsymbol{\varepsilon}_{\mathcal{M}}} \cdot \mathbf{Z}$. This covers the error directly related to the finite element model (mesh, constitutive law, etc.).

$\boldsymbol{\varepsilon}_{\widehat{\mathcal{M}}}$ was considered to be zero (Tab. 3).

4. RESULTS AND DISCUSSION

4.1. *Sensitivity analyses*

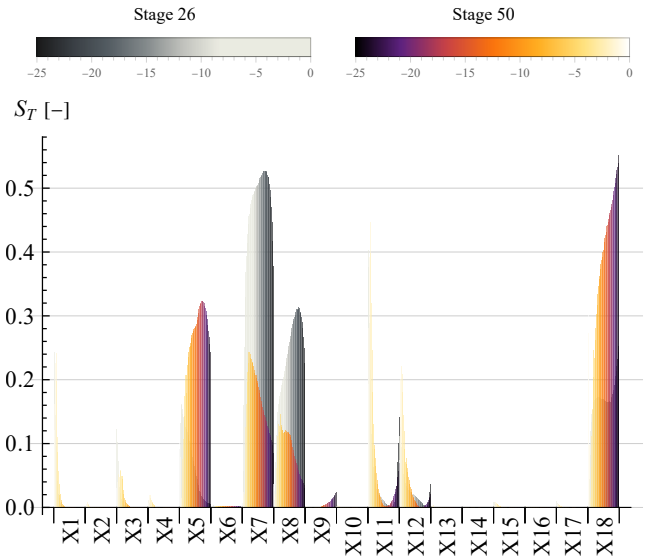

Figure 3: Total Sobol' indices for the QoI U_x at stage 26 and 50, ranging from -25 to 0 metres in depth.

The sensitivity analysis result is presented in Fig. 3. As the QoI U_x depends on the height, we chose to represent the total Sobol' indices as a gradient varying from 0 to -25 m, such as $U_x(y)$. Both stage 26 and stage 50 are shown in Fig. 3. The Sobol indices show that regardless of the selected vertical position, the variables affecting the model response are: **X1**: Young modulus of the fill layer; **X5**: Friction angle of the FC-Wurm retreat; **X7** and **X8**: Young modulus resp. Γ_{ur} of the FC-Wurn retreat; **X11** and **X12**: Young modulus resp. Γ_{ur} of the WC-Wurn retreat; **X18**: Water pressure. We also compared the total indices to the first indices, similar results were obtained. By personal choice, we judged variable X1 to be of little relevance to the study and decided to exclude it. Therefore, the remaining six parameters are kept as probabilistic variables while the others are set to their mean value. We defined these six random variables as *the prior*.

4.2. *Meta-modelling error*

The calculations presented later in this document will be performed entirely on the PCK-models. The leave-one-out errors (Allen (1974)) of the PCK are listed in Tab. 3.

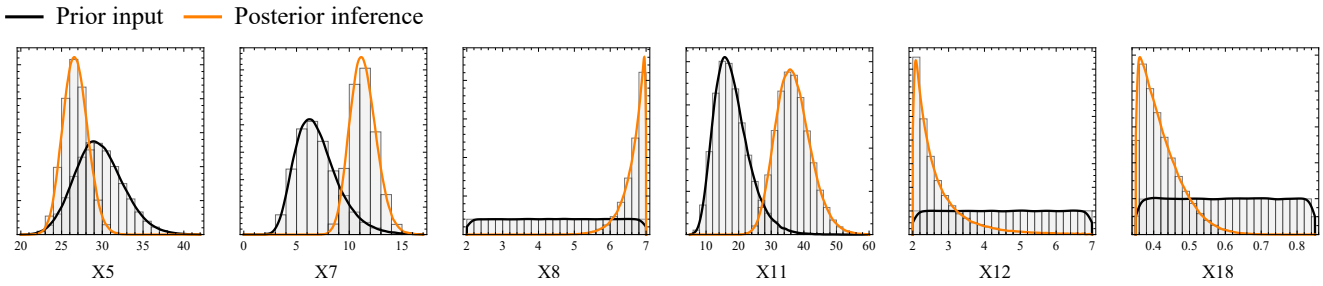

Figure 4: Bayesian-output plot showing prior and posterior distribution of model parameters.

Table 3: Leave-one-out error $LOO \times 10^{-4}$ (–).

$\widehat{\mathcal{M}}_{\text{PCK}}$	$U_{x,\text{Max}}$	U_y	M
Stage 26	6.8	4.0	2.3
Stage 50	1.2	2.2	0.5

4.3. Bayesian inversion

Figure 6: Picture showing stage 26 of the excavation.

Bayesian inversion was performed at stage 26 when the excavation was as shown in Fig. 6. Using inversion techniques described in section 2.5, the prior refinement yields the result shown in Fig. 4. The Gelman-Rubin criterion (convergence assessing method introduced by Gelman and Rubin (1992)) yielded a value of $\hat{R}^p = 1.05$ which confirms the convergence of the MCMC solver. Inference on the output-sampling set showed that variables X5, X7, X8, X11 and X12 could be associated with Lognormal and truncated Lognormal distributions, whereas X18 was identified to be a truncated Gaussian. As shown in Fig. 7, the deformability parameters show a noticeable tendency to increase the system's stiffness. Moreover, the friction angle of the FC-Wurm retreat switched from a 30° to a 26° mean. We interpreted this result as follows: our model is steady-state, so the algorithm was learning to represent the deformations measured in situ by converting the long-term into short-term parameters by increasing the Young moduli and by decreasing the friction angle. By introducing the water pressure via the fluid density, we also noted that the physical interpretation of the posterior of the geomechanical parameters is difficult.

Fig. 7 shows the difference between prior predictions at stage 26 and the posterior prediction after input parameters calibration via Maximum A posteriori Probability (MAP). In the project schedule, additional measures are foreseen at stage 33. Although not presented in this study, these measurements will allow refinement and validation of the result obtained at stage 26.

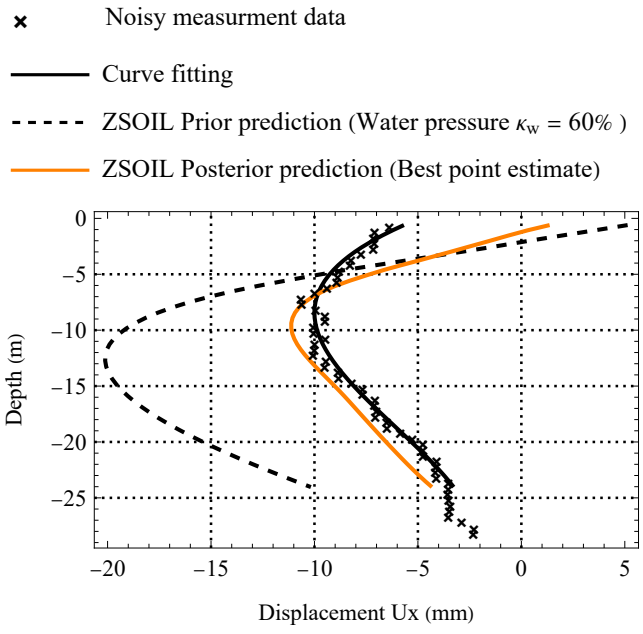

Figure 7: Prior prediction and MAP at stage 26.

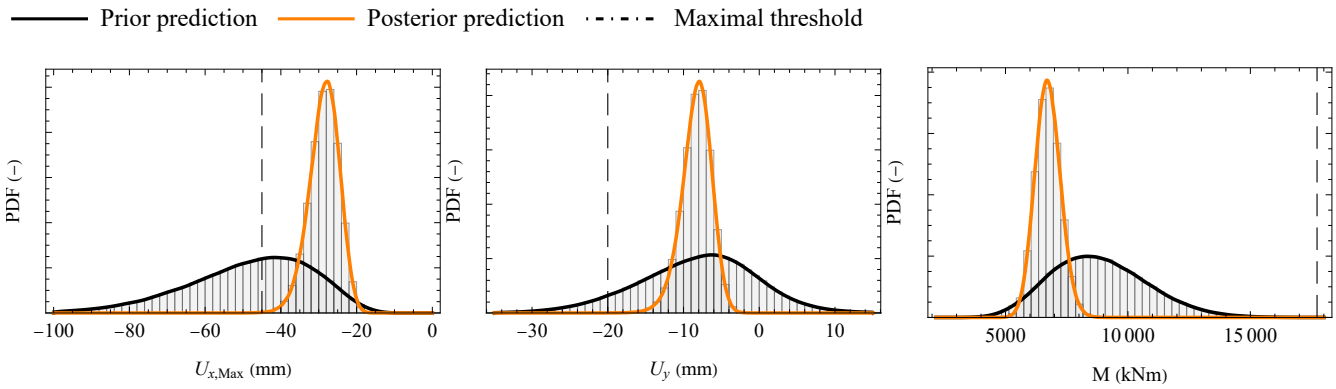

(a) Maximal x-displacement (b) Conduit settlement (c) Bending moment

Figure 5: Probability density function of the QoI at finale stage 50 with receptive maximal threshold.

4.4. Reliability analyses

Considering Eq. (7), failure criteria must be defined to perform a reliability analysis. For the current project, the following maximal thresholds in absolute value have been defined :

Table 4: List of the failure functions $g(\boldsymbol{X})$.

	U_x (mm)	U_y (mm)	M (kNm)
$g(\boldsymbol{X})$	$45 - \lvert U_{x,\mathrm{Max}} \rvert$	$20 - \lvert U_y \rvert$	$M_{Rd} - \lvert M \rvert$

where $M_{Rd} = 17'700$ (kNm) is the bending strength of the 4.32 meters width slice defined as design value.

Propagating the prior and the posterior uncertainties led to the result shown in Fig. 5. The distributions shown in the same figure were obtained by running 10^5 model evaluations and are to consider only for visualization purposes. Probabilities of failure $P_{f,i}$ were obtained with 10^7 model evaluations. According to the fixed failure functions, the probabilities of failure listed in Tab. 5 were computed.

Table 5: Probabilities of failure in % according to the thresholds fixed in Tab. 4.

	U_x (mm)	U_y (mm)	M (kNm)
Prior	53.0	7.3	0.0026
Posterior	0.05	0.0036	$< 10^{-5}$

Given the failure probabilities obtained in Tab. 5, the suppression of the fourth row of struts initially planned can be proposed. However, at the time of writing this article, we were waiting for new measurements to confirm the model's predictions.

5. CONCLUSION

The present contribution proposes a Bayesian analysis based on the horizontal deflection of a concrete diaphragm wall. After having performed a sensitivity analysis, meta-modelling techniques, Bayesian updating and reliability analyses, the principal findings of the study are listed as follows:

(1) Impacting factors on the quantities of interest are principally located in the few consolidated Wurm retreat with weak strength and deformability properties.

(2) Our numerical model has learned to represent reality with sufficient accuracy. However, the physical interpretation of the posterior variables is difficult due to the nature of the original model (steady-state).

(3) The posterior failure probabilities were sufficiently low to allow the proposal of design optimization, i.e., the suppression of the fourth struts row.

As the project stands, the next task will be to verify the predictions using the new measurements from stage 33. We consider this validation to be mandatory in order to guarantee structural safety and serviceability thresholds. A step forward would be to reconsider our numerical model by turning it into a fully coupled consolidation model.

ACKNOWLEDGEMENTS

The authors would like to thank **Marie Dupays**, **Jérémie Crisinel** and **Scott Favre** from De Cerenville Géotechnique SA for the supply of the measurement data as well as the various photos and information on the project, thus enabling the writing of this document.

ROLE OF THE FUNDING SOURCE

This study has been financed by the "Ingénierie et d'Architecture" domain of HES//SO, University of Applied Sciences Western Switzerland, which is acknowledged.

REFERENCES

Allen, D.M., 1974. The Relationship Between Variable Selection and Data Agumentation and a Method for Prediction. Technometrics 16, 125–127. doi:10.1080/00401706.1974.10489157.

Commend, S., Geiser, F., Crisinel, J., 2004. Numerical simulation of earthworks and retaining system for a large excavation. Advances in Engineering Software 35, 669–678. doi:https://doi.org/10.1016/j.advengsoft.2003.10.011.

Cudny, M., Truty, A., 2020. Refinement of the Hardening Soil model within the small strain range. Acta Geotechnica 15, 2031–2051. doi:10.1007/s11440-020-00945-5.

Gelman, A., Rubin, D.B., 1992. Inference from Iterative Simulation Using Multiple Sequences. Statistical Science 7, 457 – 472. doi:10.1214/ss/1177011136. publisher: Institute of Mathematical Statistics.

Marelli, S., Sudret, B., 2014. UQLab: A Framework for Uncertainty Quantification in Matlab , 2554–2563doi:10.1061/9780784413609.257. publisher: American Society of Civil Engineers.

Obrzud, R., Truty, A., 2010. The hardening soil model-a practical guidebook Z_Soil. Technical Report PC100701.

Phoon, K.K., Ching, J. (Eds.), 2018. Risk and Reliability in Geotechnical Engineering. 0 ed., CRC Press. doi:10.1201/b17970.

Pictet Group, 2023. Campus Pictet de Rochemont.

de Rocquigny, E., Devictor, N., Tarantola, S., 2008. Uncertainty in industrial practice: a guide to quantitative uncertainty management. John Wiley & Sons.

Schöbi, R., 2019. Surrogate models for uncertainty quantification in the context of imprecise probability modelling. Technical Report. ETH Zurich. doi:10.3929/ETHZ-B-000373587.

Sobol, I., 2001. Global sensitivity indices for nonlinear mathematical models and their Monte Carlo estimates. Mathematics and Computers in Simulation 55, 271–280. doi:10.1016/S0378-4754(00)00270-6.

Sudret, B., 2007. Uncertainty propagation and sensitivity analysis in mechanical models – Contributions to structural reliability and stochastic spectral methods .

TG-C3, 2023. Reliability-based methods for geotechnical design and assessment. Guideline document for the next-generation Eurocodes. Technical Report CEN/TC250/SC7/TG-C3.

Wagner, P.R., Nagel, J., Marelli, S., Sudret, B., 2021. UQLab user manual – Bayesian inversion for model calibration and validation. Technical Report. Chair of Risk, Safety and Uncertainty Quantification, ETH Zurich, Switzerland.

ZSOIL, 2023. A Windows-Based Tool offering a unified approach to numerical simulation of soil and rock mechanics, above & underground structures, excavations, soil-structure interaction and underground flow, including dynamics, thermal and moisture migration analysis. GeoDev SARL.